NASA TECHNICAL NOTE

NASA TN D-2978

NASA TN D-2978

c. 1

TECH LIBRARY KAFB, NM
0079940

LOAN COPY: RE
AFWL (WLI
KIRTLAND AFB,

EFFECT OF ADDING TUNGSTEN FILLER MATERIAL TO BERYLLIA MAGNESIA THERMAL STORAGE MATERIAL IN A SOLAR THERMIONIC POWER SYSTEM

by William J. Bifano and James J. Ward

Lewis Research Center
Cleveland, Ohio

NATIONAL AERONAUTICS AND SPACE ADMINISTRATION • WASHINGTON, D. C. • SEPTEMBER 1965

TECH LIBRARY KAFB, NM
0079940

EFFECT OF ADDING TUNGSTEN FILLER MATERIAL TO BERYLLIA MAGNESIA THERMAL STORAGE MATERIAL IN A SOLAR THERMIONIC POWER SYSTEM

By William J. Bifano and James J. Ward

Lewis Research Center
Cleveland, Ohio

NATIONAL AERONAUTICS AND SPACE ADMINISTRATION

For sale by the Clearinghouse for Federal Scientific and Technical Information
Springfield, Virginia 22151 – Price $2.00

EFFECT OF ADDING TUNGSTEN FILLER MATERIAL TO BERYLLIA MAGNESIA THERMAL STORAGE MATERIAL IN A SOLAR THERMIONIC POWER SYSTEM

by William J. Bifano and James J. Ward
Lewis Research Center

SUMMARY

An investigation of the effect on system specific weight of adding tungsten filler material to beryllia magnesia (3 BeO - 2 MgO) thermal storage material in a solar thermionic power system is presented. A one-dimensional steady-state heat-transfer analysis is employed to determine system performance. A transient heat-transfer analysis and a discussion of thermal control requirements and variations in electrical output power during an orbit are included in the appendixes.

The results indicate that the addition of tungsten to the 3 BeO - 2 MgO does not lower the specific weight of the system, although small amounts may be added to relieve thermal stresses, for example, without increasing the specific weight significantly. In addition, it is found that by means of a variable generator aperture, an output power variation of less than 6 percent can be maintained through a light-dark cycle for a system designed for a maximum cavity temperature of 2200° K operating with a fixed load resistance.

INTRODUCTION

For orbital applications, solar energy power systems require a means of maintaining electrical output power during the dark period of an orbit. Rechargeable electrical storage batteries having high-cycle life have been used for this purpose.

For thermal power systems, an alternate technique for continuously maintaining power involves the use of thermal energy storage (TES) materials. During the light period of an orbit, a portion of the solar energy delivered to the system would be absorbed by the storage material and be made available to the energy converter during the dark period. It is expected that the use of such materials will result in net energy storage capacities in excess of the values currently being attained with batteries. In addition, thermal cycling of the energy conversion devices would be eliminated.

Several materials that exhibit high specific energy and have high melting points have been considered for solar thermionic applications. However, because these materials are relatively poor heat conductors, it has been proposed that refractory metal filler materials be added to improve heat-transfer characteristics. Studies of solar thermionic systems employing the compound 3 BeO - 2 CaO (melting point, 1685° K; heat of fusion, 116 W-hr/lb) and the eutectic Al_2O_3 - 4 BeO - 4MgO (melting point, 1910° K; heat of fusion, 160 W-hr/lb) as energy storage materials (ref. 1) have indicated that the addition of a limited amount of metal filler (molybdenum in this case) results in a reduction in system specific weight. The minimum specific weight, which occurs when 10 percent filler, by volume, is present, was found to be 285 and 185 pounds per kilowatt for the 3 BeO - 2 CaO and Al_2O_3 - 4 BeO - 4 MgO systems, respectively.

The study reported herein has been undertaken to determine the effect on system specific weight of adding tungsten filler to 3 BeO - 2 MgO thermal storage material (melting point, 2145° K, heat of fusion, 264 W-hr/lb) in a solar thermionic application. System components considered in the analysis (e. g., thermionic converters, generator support structures, etc.) are similar to those used in the Solar Energy Thermionic (SET) System design (ref. 2).

In estimating system performance, the thermal energy delivered to the generator is considered to be constant over the entire orbit, and a one-dimensional steady-state heat-transfer analysis is employed. However, a transient heat-transfer analysis, as well as thermal control requirements and variations in electrical output power during an orbit, are considered in the appendixes.

METHOD OF ANALYSIS

System Description

A schematic diagram of the TES solar thermionic generator considered in this study is shown in figures 1(a) and (b). The electrical output power of the generator is supplied by four thermionic converters, each of which is mounted on the outer wall of a metal container of beryllia magnesia (3 BeO - 2 MgO). The generator cavity is defined by the inner walls of the generator quadrants. (A generator "quadrant" consists of one beryllia magnesia container plus one-fourth of the aperture and rear walls, as shown in fig. 1(c).) Tungsten is used as the containment material, and each container is assumed to have an outer wall thickness of 40 mils; the remaining walls of the quadrant have a thickness of 20 mils. Tantalum radiation shields are provided to limit the heat loss by

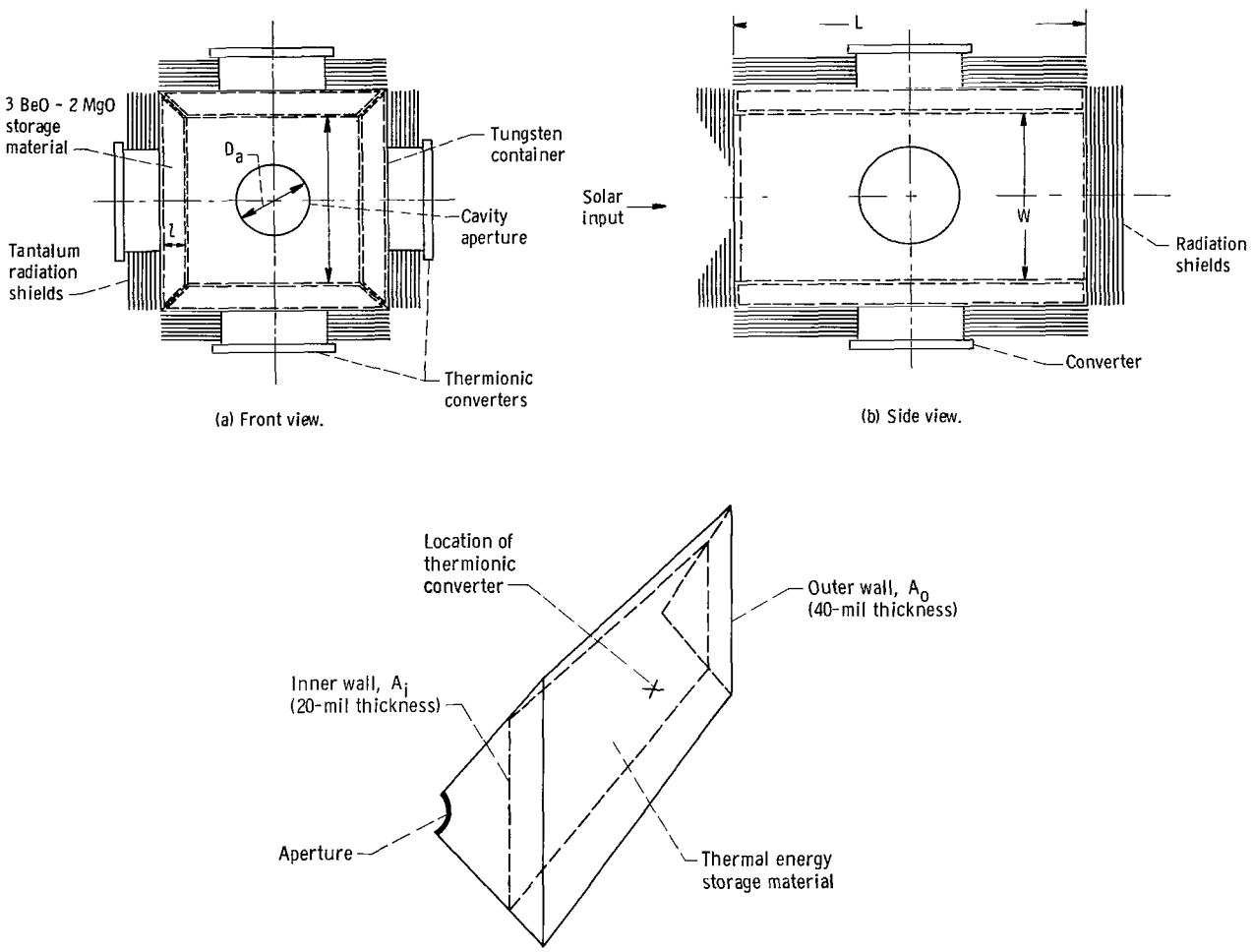

Figure 1. - Schematic diagram of four converter thermal energy storage generator with length to width ratio L/W = 2.

radiation from the exterior walls of the quadrant to 10 percent of the thermal power reaching the outer wall of the container. An aperture door is required to eliminate reradiation losses during the dark period. The cavity aperture is located in the focal plane of a one-piece, parabolic, solar concentrator having a 5-foot diameter.

Thermal Considerations

A thermal energy storage solar thermionic system orbiting the Earth, alternately operating in sunlight and shadow, will experience continuously varying internal temperatures and heat fluxes. The variations in cavity and emitter temperature that occur during one orbit in an ideal system are illustrated schematically in figure 2.

At the end of the light period the liquid-solid interface of the melting storage mate-

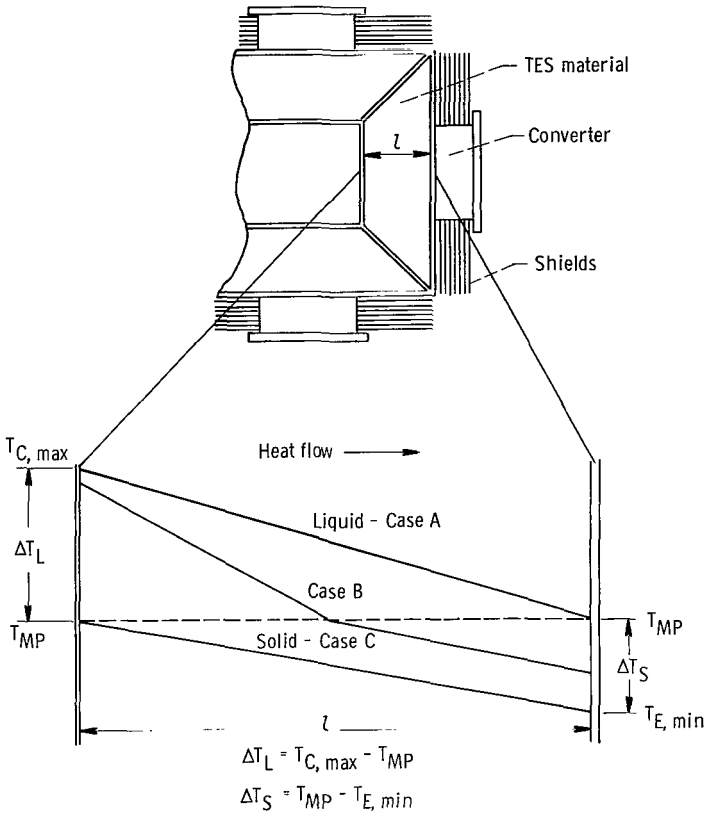

Figure 2. - Thermal storage-material temperature distribution.

rial will arrive at the outer wall of the container to which is attached the emitting electrode of a thermionic converter (Case A, fig. 2). At this time, the cavity wall temperature will be at its maximum value ($T_C = T_{C, max}$), and the emitter temperature will reach the TES material melting point ($T_E = T_{MP}$). (A complete list of symbols used is presented in appendix A.) The resultant temperature difference across the liquid TES material is designated ΔT_L

$$\Delta T_L = T_{C, max} - T_{MP} \qquad (1)$$

As the system continues into the dark period of the orbit, the liquid-solid interface of the storage material moves toward the cavity wall. At an intermediate point in the dark period, the temperature gradient would be of the type shown in Case B, figure 2. The interface will arrive at the cavity wall just as the system emerges from the Earth's shadow (Case C, fig. 2). At this time, the cavity wall will be at the melting point of the storage material ($T_C = T_{MP}$), and the emitter temperature will reach its minimum value ($T_E = T_{E, min}$). The resulting temperature difference across the solid TES material is designated ΔT_S.

$$\Delta T_S = T_{MP} - T_{E, min} \qquad (2)$$

In estimating the overall system performance, it was assumed that the cavity was operating at its maximum temperature ($T_C = T_{C, max}$) during the light period and that the emitter was operating at its minimum temperature ($T_E = T_{E, min}$) throughout the entire orbit. Under these assumptions, the available solar energy, as well as the heat flux required by the converter is constant for a given cavity temperature.

The analyses presented in appendixes B and C indicate that the effect on system performance due to varying temperatures and thermal inputs is not significant. Although the operating points used in the appendix do not correspond to design points for an actual system, they were selected to provide a conservative performance estimate.

A one-dimensional steady-state heat-transfer analysis is employed to (1) establish the relation between ΔT_L and ΔT_S, and (2) to determine the TES material cross-sectional area A_{cs} and thickness l required to satisfy these relations.

At the end of the light period, assuming that heat is stored only at the liquid-solid interface, the thermal power from the receiver Q_W is related to ΔT_L through the heat conduction equation

$$Q_W = \frac{k_L A_{cs} \times \Delta T_L}{l} \tag{3a}$$

where

k_L thermal conductivity of liquid TES material

A_{cs} logarithmic-mean-area of TES material container (i.e., $A_{cs} = (A_o - A_i)/\ln(A_o/A_i)$, where A_o and A_i are the outer and inner wall areas, respectively, as shown in fig. 3)

l thickness of TES material

Also, at the end of the dark period, the thermal power that reaches the emitter wall Q_E is related to ΔT_S through the heat conduction equation

$$Q_E = \frac{k_S A_{cs} \times \Delta T_S}{l} \tag{3b}$$

where k_S is the thermal conductivity of the solid TES material.

The fraction of the thermal power Q_W that reaches the emitter wall Q_E is equal to $t_l/(t_l + t_d)$ where t_l and t_d are the orbit light and dark time, respectively. For a 300-mile circular orbit

$$Q_E = 0.61\, Q_W \tag{4}$$

Taking k_S equal to k_L and dividing equation (3a) by equation (3b) results in

$$\frac{Q_W}{Q_E} = \frac{\Delta T_L}{\Delta T_S} = 1.64 \tag{5}$$

In regard to the thermal conductivity ratio k_L/k_S, there is no experimental conductivity data available for 3 BeO - 2 MgO. However, data obtained for similar materials, for example 3 BeO - 2 CaO, show that the liquid conductivity is greater than the solid conductivity. Preliminary calculations performed with values of k_L/k_S from

1 to 4 indicated that the general conclusions of the study were not dependent on this parameter. Therefore, a conductivity ratio of 1 was used in determining system performance.

If the heat capacity effects are neglected, the required mass of TES material is related to the total energy stored $Q_E t_d$ by the following equation:

$$Q_E t_d = mH_S = \rho_S \bar{A}\, \ell H_S \tag{6}$$

where

m mass of TES material

H_S heat of fusion of TES material

ρ_S density of TES material

$\bar{A}$ arithmetic-mean-area of TES material (i.e., $\bar{A} = (A_o + A_i)/2$).

(In this analysis, the arithmetic mean area $\bar{A}$ and logarithmic mean area A_{cs} are considered equivalent. When the ratio A_o/A_i does not exceed 2, as is generally the case in this study, the arithmetic mean area is within 4 percent of A_{cs}.) Solving for ℓ in equation (6) then and substituting into equation (3b) give

$$Q_E = \frac{k_S A_{cs}\, \Delta T_S}{\dfrac{Q_E t_d}{H_S \rho_S A_{cs}}} \tag{7}$$

The required TES material cross-sectional area is therefore

$$A_{cs} = \left(\frac{Q_E^2 t_d}{\rho_S H_S k_S\, \Delta T_S} \right)^{1/2} \tag{8}$$

The corresponding thickness of TES material is found by solving for ℓ in equation (3b)

$$\ell = \frac{k_S A_{cs}\, \Delta T_S}{Q_E} \tag{9}$$

Equations (8) and (9) may be modified to describe the system when various combinations of TES material and metal filler are used to increase thermal conductivity. If the metal filler material is added in the form of rods that are alined along paths of constant thermal flux, as shown in the schematic diagram of figure 3, averaging techniques may

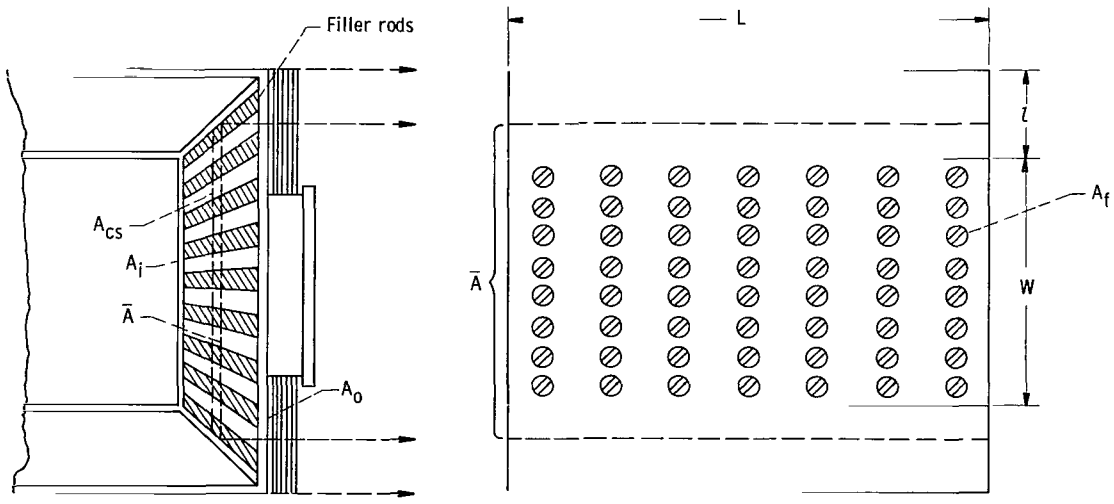

Figure 3. - Schematic showing addition of filler to thermal storage material.

be used to obtain property values for the filler-storage material composite. In calculations involving filler material, it is convenient to use the factor α, which is defined as the ratio of storage material to total material (storage and filler) on a volumetric basis. The physical properties of storage-filler combinations are expressed as functions of α in the following equations:

$$\alpha = \frac{v_s}{v_s + v_f} = \frac{\bar{A}_s}{\bar{A}_s + \bar{A}_f} \tag{10}$$

$$\rho_t = \frac{\rho_s \bar{A}_s + \rho_f \bar{A}_f}{\bar{A}_s + \bar{A}_f} = \rho_s \alpha + \rho_f (1 - \alpha) \tag{11}$$

$$k_t = \frac{k_s \bar{A}_s + k_f \bar{A}_f}{\bar{A}_s + \bar{A}_f} = k_s \alpha + k_f (1 - \alpha) \tag{12}$$

$$H_t = \frac{\rho_s \bar{A}_s H_s}{\rho_s \bar{A}_s + \rho_f \bar{A}_f} = \frac{\rho_s \alpha H_s}{\alpha \rho_s + \rho_f (1 - \alpha)} \tag{13}$$

where

ρ density

k thermal conductivity

H heat of fusion

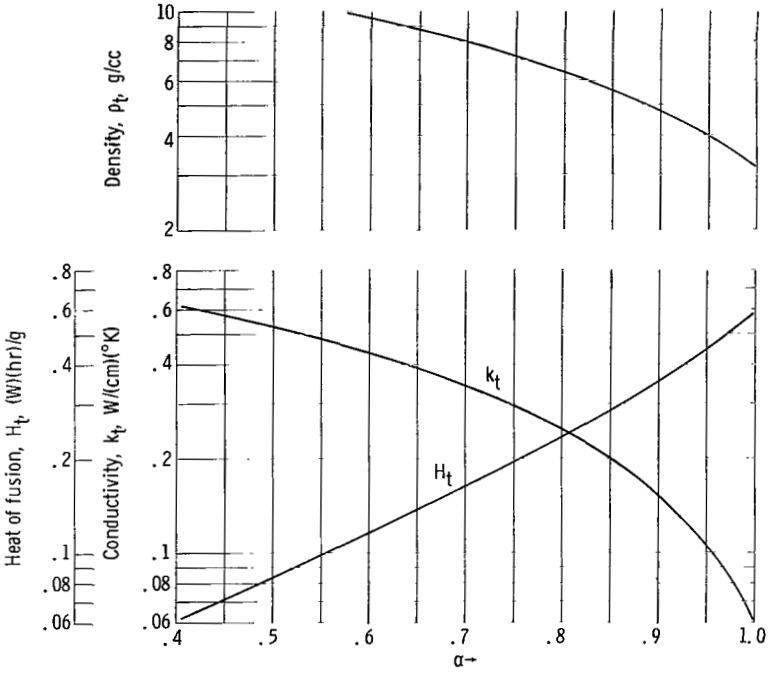

Figure 4. - Conductivity, density, and heat of fusion plotted against α for 3 BeO - 2 MgO - tungsten mixture.

TABLE I. - PHYSICAL PROPERTY VALUES

Material	Physical property	Value	Source
3 BeO - 2 MgO	Storage-material density, ρ_s, g/cc	3.2	Ref. 1
	Storage-material thermal conductivity, k_s, W/(cm)(°K)	0.06	Estimated value
	Storage-material heat of fusion, H_s, (W)(hr)/g	0.581	Ref. 1
Tungsten	Filler-material density, ρ_f, g/cc	19.3	Ref. 7
	Filler-material thermal conductivity, k_f, W/(cm)(°K)	1.0	Ref. 7
Tantalum	Density, ρ, g/cc	16.6	Ref. 7

and s, f, and t are subscripts referring to storage material, filler material, and total combination, respectively. The values of all physical properties used in this study are given in table I.

Plots of ρ_t, k_t, and H_t against α are presented in figure 4 for beryllia magnesia tungsten combinations. As indicated in the figure, the increase in thermal conductivity k_t resulting from the addition of filler is accompanied by a corresponding increase in density ρ_t and decrease in heat of fusion H_t.

The cross-sectional area of the storage-filler combination may now be expressed by writing equation (8) in terms of α

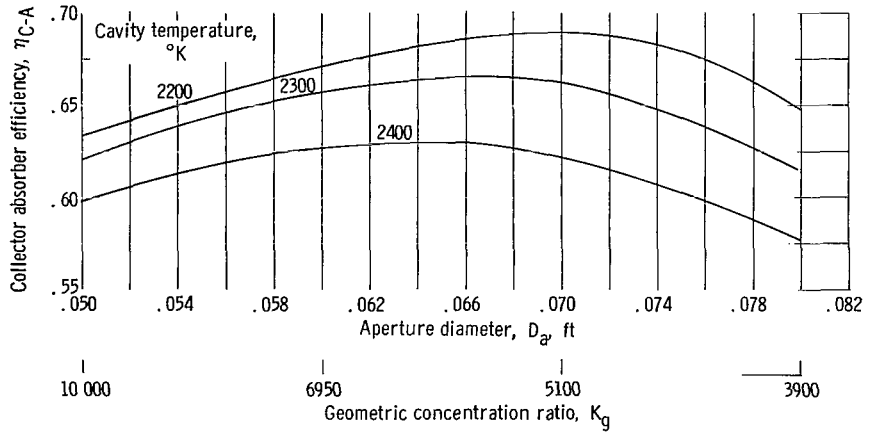

Figure 5. - Collector absorber efficiency plotted against aperture diameter and geometric concentration ratio. Misorientation angle $\beta = 0$; reflectivity $r = 0.9$.

$$A_{cs} = \left\{ \frac{Q_E^2 t_d}{\alpha\left[k_s\alpha + k_f(1 - \alpha)\right]\rho_s H_s \Delta T_S} \right\}^{1/2} \tag{14}$$

The corresponding thickness l becomes

$$l = \frac{k_t A_{cs} \Delta T_S}{Q_E} = \frac{\left[k_s\alpha + k_f(1 - \alpha)\right] A_{cs} \Delta T_S}{Q_E} \tag{15}$$

Now by specifying a maximum cavity temperature, the thermal power from the receiver Q_W is determined from solar collector-absorber performance data (discussed in the following section). The thermal power reaching the emitter wall Q_E and the temperature difference across the solid TES material ΔT_S are then determined from equations (1) to (5). The required cross-sectional area and thickness of the TES material is then calculated from equations (14) and (15), respectively, for a given value of α.

Solar Collector Performance

Solar collector performance curves used in this study were calculated for a parabolic collector having a rim angle $\theta = 60^\circ$, a reflectivity $r = 0.9$, and a normal distribution of collector surface errors with a standard deviation $\sigma' = 1/8^\circ$. A digital computer was used to predict the collector-absorber efficiency η_{C-A} as a function of cavity temperature. Corrections are included for energy losses due to reradiation, assuming a cavity having blackbody characteristics. A plot of collector-absorber efficiency against concentration ratio K_g (ratio of collector area to aperture area) is shown in

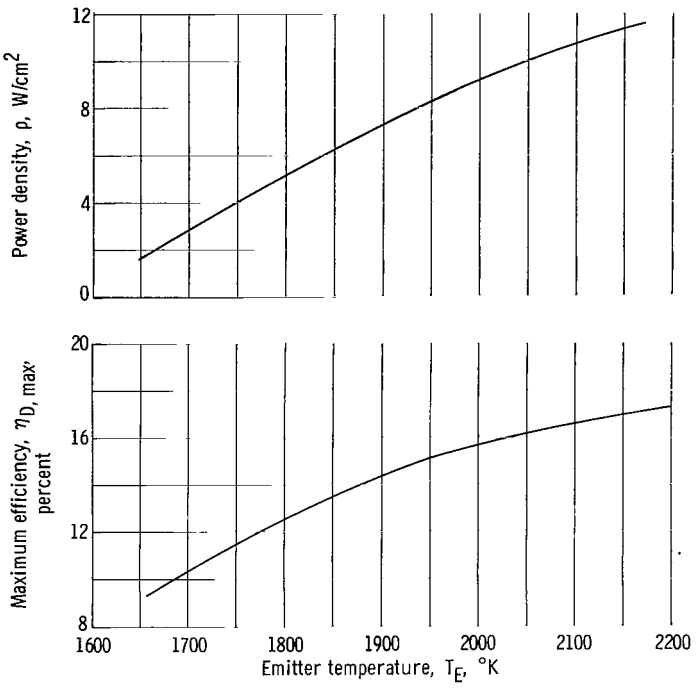

Figure 6. - Power density and maximum efficiency plotted against emitter temperature for variable-spaced planar diode (rhenium emitter - molybdenum collector).

figure 5 for cavity temperatures of 2200° , 2300° , and 2400° K and zero collector misorientation $\beta = 0$. Also presented on the abscissa are the corresponding aperture diameters for a 5-foot-diameter concentrator. For a given concentration ratio, the decrease in collector-absorber efficiency, which occurs with increasing cavity temperature, is due to reradiation losses from the cavity. The optimum concentration ratios (i. e., 5000 to 6000) result in collector-absorber efficiences in the range of 60 to 70 percent.

In sizing the cavity, the optimum aperture diameters, ranging from 0. 070 foot at a cavity temperature of 2200° K to 0. 065 foot at a cavity temperature of 2400° K, were used. The available thermal power is then found from the collector performance curves, assuming a solar constant of 130 watts per square foot.

Thermionic Converter Performance

In determining the generator output power, thermionic converter performance data obtained with a variable-spacing diode having a rhenium emitter and a molybdenum collector were used (ref. 3). Figure 6 presents maximum diode efficiency $\eta_{D, max}$ and corresponding power density p against emitter temperature for the aforementioned diode. Taking an outer wall radiation loss of 0. 1 Q_E, the emitter area corresponding to a given emitter temperature may be found.

$$A_E = \frac{0.9\, Q_E}{\frac{p}{\eta_{D, max}}} \tag{16}$$

The generator efficiency η_G is given by

$$\eta_G = \frac{pA_E}{Q_E} \tag{17}$$

while the system efficiency η_{sy} is

$$\eta_{sy} = \eta_{C\text{-}A}\eta_G \tag{18}$$

Component Specific Weight

The following components are considered in calculating specific weight: (1) solar collector, (2) thermionic converters (including the radiator required to reject the waste heat from the anode collector), (3) generator support structure, (4) TES material, (5) TES material container, and (6) radiation shielding. System components not included in specific weight calculations such as power conditioning equipment, collector orientation hardware, and vehicle support structure will affect the level of the specific weight curves; however, the trends and conclusions will remain unchanged.

For this analysis, a collector weight of 0.5 pound per square foot is assumed. The converter specific weight (including radiator) is scaled from the SET system diode weight (i.e., 0.22 lb/cm^2 of emitter area) (ref. 2). The generator support structure specific weight is taken as 0.25 of the collector specific weight.

The TES material specific weight is calculated using the following equation:

$$SW_{TES} = \frac{2.2\, t_d}{\eta_G H_t} \tag{19}$$

The container specific weight is calculated for a tungsten container assuming an outer wall thickness of 40 mils and 20-mil-thick walls elsewhere.

The thermal shields are considered to be thin parallel plates arranged such that end losses may be neglected and the heat transfer between shields is solely due to radiation. For this case, assuming a sink temperature of 0° K, the number of shields n required to limit the heat loss by radiation from the outer wall to 0.1 Q_E is

$$n = \frac{\sigma(T_E^4 - T_n^4)A_r}{\left(\frac{2}{\epsilon} - 1\right)(0.1\, Q_E)} \tag{20}$$

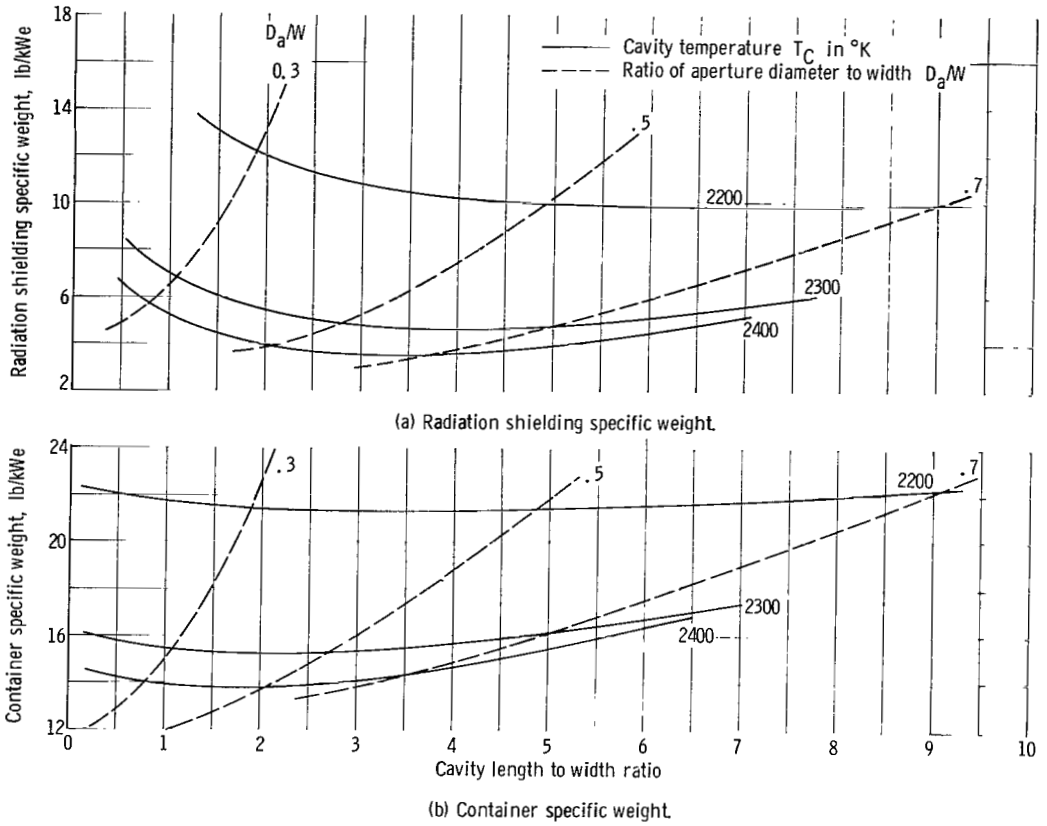

(a) Radiation shielding specific weight.

(b) Container specific weight.

Figure 7. - Radiation shielding and container specific weight plotted against cavity length to width ratio for $\alpha = 1$.

Or, since $T_n^4 = \dfrac{0.1\,Q_E}{\sigma \epsilon A_r}$,

$$n = \frac{\sigma \epsilon A_r T_E^4 - 0.1\,Q_E}{(2 - \epsilon)(0.1\,Q_E)} \tag{21}$$

where

T_n temperature of n^{th} shield

A_r radiating area

ϵ emissivity of shield material

σ Stefan-Boltzmann constant

Weight calculations are based on the use of 0.3-mil-thick tantalum shields having an emissivity of 0.3.

Plots of shielding and container specific weight against cavity length to width ratio L/W for $\alpha = 1$ are shown in figure 7. (These are the only component weights directly

TABLE II. - CALCULATED VALUES OF THERMAL ENERGY STORAGE - SOLAR THERMIONIC SYSTEM PERFORMANCE

α	Cross-sectional area, A_{cs}, cm^2	Thickness, l, cm	Emitter area, A_E, cm^2	Converter power output, pA_E, W	Generator power output, $4pA_E$, W	Cavity width, W_C, cm	Outer wall area of absorber, A_o, cm^2	Inner wall area of absorber, A_i, cm^2	Collector specific weight, lb/kWe	Thermal storage-material specific weight, lb/kWe	Thermionic converter specific weight, lb/kWe	Generator support specific weight, lb/kWe	Thermal storage-material container specific weight, lb/kWe	Radiation shield specific weight, lb/kWe	Total specific weight, lb/kWe	Generator efficiency, η_G, percent	System efficiency, η_{sy}, percent	Collector-absorber efficiency, η_{C-A}, percent
Cavity temperature, 2400° K; optimum aperture diameter, 1.98 cm; net input thermal power, 1610 W; wall thermal power, 402 W; emitter temperature, 1990° K; emitter thermal power, 245 W; diode power density, 9 W/sq cm; diode efficiency, 15.6 percent																		
1.0	44.8	1.71	3.81	34.3	137.0	4.02	59.8	32.4	71.7	17.2	22.8	17.9	13.8	4.0	147.4	14.0	8.82	63.0
0.9	29.6	2.80	3.81	34.3	137.0	2.90	49.3	16.8	71.7	28.5	22.8	17.9	12.4	3.73	156.5	14.0	8.82	63.0
0.7	22.5	4.98	3.81	34.3	137.0	2.00	48.0	8.0	71.7	67.3	22.8	17.9	12.6	5.13	196.0	14.0	8.82	63.0
Cavity temperature, 2300° K; optimum aperture diameter, 2.05 cm; net input thermal power, 1700 W; wall thermal power, 425 W; emitter temperature, 2050° K; emitter thermal power, 259 W; diode power density, 10 W/sq cm; diode efficiency, 16.2 percent																		
1.0	61.0	1.33	3.77	37.7	150.8	4.95	75.4	49.0	65.4	16.5	20.5	16.3	15.2	5.5	139.0	14.55	9.69	66.6
0.9	40.0	2.18	3.77	37.7	150.8	3.60	57.3	26.0	65.4	27.6	20.5	16.3	12.4	3.92	146.0	14.55	9.69	66.6
0.7	30.5	3.90	3.77	37.7	150.8	2.70	56.0	14.6	65.4	64.0	20.5	16.3	13.9	6.25	186.0	14.55	9.69	66.6
0.5	29.0	5.60	3.77	37.7	150.8	2.30	62.0	10.6	65.4	116.8	20.5	16.3	17.1	11.5	248.0	14.55	9.69	66.6
Cavity temperature, 2200° K; optimum aperture diameter, 2.13 cm; net input thermal power, 1760 W; wall thermal power, 440 W; emitter temperature, 2111° K; emitter thermal power, 268 W; diode power density, 10.9 W/sq cm; diode efficiency, 16.6 percent																		
1.0	105.0	0.79	3.67	40.0	160.0	6.90	117.0	95.2	61.5	16.1	18.9	15.4	21.4	12.0	145.0	14.9	10.3	69.0
0.9	69.5	1.30	3.67	40.0	160.0	5.30	84.0	56.2	61.5	26.6	18.9	15.4	15.9	6.84	145.0	14.9	10.3	69.0
0.7	53.0	2.32	3.67	40.0	160.0	4.25	75.5	36.1	61.5	60.2	18.9	15.4	15.3	6.84	178.0	14.9	10.3	69.0
0.5	50.4	3.34	3.67	40.0	160.0	3.80	79.5	27.4	61.5	113.0	18.9	15.4	16.9	9.27	235.0	14.9	10.3	69.0

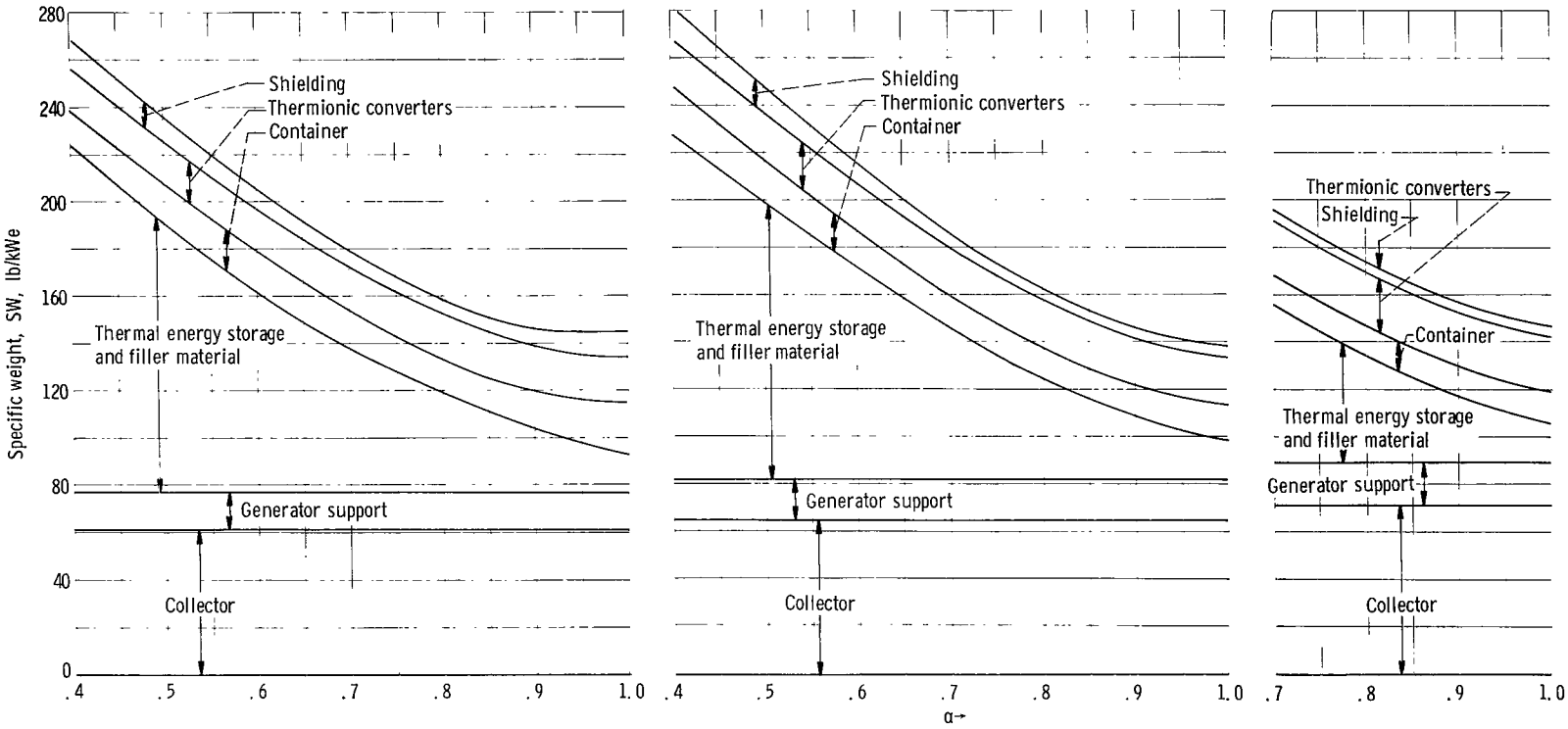

(a) Cavity temperature T_C = 2200° K.

(b) Cavity temperature T_C = 2300° K.

(c) Cavity temperature T_C = 2400° K.

Figure 8. - Specific weight plotted against α for length to weight ratio L/W = 2 and various cavity temperatures.

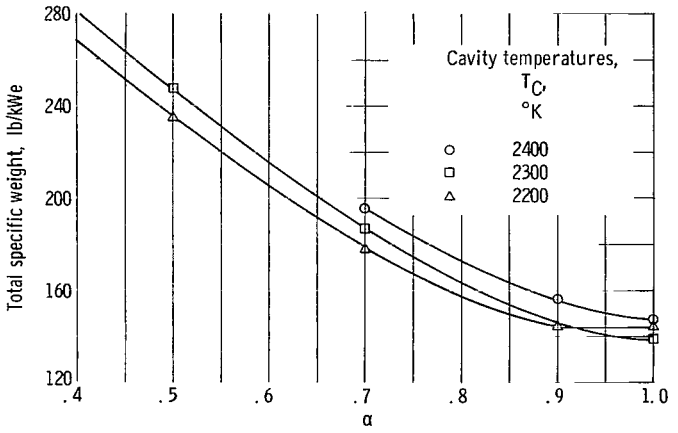

Figure 9. - Total specific weight plotted against α for length to width ratio L/W = 2.

dependent on L/W.) Since these weights are relatively insensitive to changes in L/W, an arbitrary value of L/W = 2 was chosen for the study, resulting in aperture diameter to cavity width ratios D_a/W between 0.3 and 0.5 for cavity temperatures of interest (i.e., 2200° to 2400° K). According to reference 4, an absorber having a ratio of aperture area to interior area of less than 0.03 approximates a blackbody. For the absorber used in the present study (L/W = 2), this ratio is found to be 0.019, 0.0137, and 0.0073 for cavity temperatures of 2200°, 2300°, and 2400° K, respectively. The choice of L/W = 2 is therefore consistent with the assumptions involved in calculating the collector-absorber performance.

Values of component specific weight calculated for various cavity temperatures and storage-filler combinations are presented in table II.

RESULTS AND DISCUSSION

Plots of component specific weight against α for each of the three cavity temperatures, 2200°, 2300°, and 2400° K (figs. 8(a), (b), and (c), respectively) indicate the following trends. In general, total system specific weight exhibits a sharp decrease as α increases from 0.5 to 0.8, tending to level off at $\alpha = 0.9$. Between 0.9 and 1.0, the weight is essentially constant for the 2200° K case whereas for 2300° and 2400° K, the weight continues to decrease slightly. In figure 8(c), T_C = 2400° K, specific weights for α less than 0.7 have not been included since the cavity width W calculated for this case is less than the optimum aperture diameter when L/W = 2. Although this situation could be remedied by choosing a lower value of L/W at this cavity temperature, no additional calculations are included.

A summary curve of total system specific weight against α for T_C = 2200°, 2300°, and 2400° K is shown in figure 9. Although the minimum specific weight of 139 pounds per kilowatt electric occurs at T_C = 2300° K, $\alpha = 1.0$, the maximum variation in weight over the range of temperatures examined is only 6 percent at $\alpha = 1$. In general, this situation exists throughout the entire range of α's. Again note that, at 2400° K, specific

weights are not presented for $L/W = 2$ since the calculated value of D_a is greater than W.

Although it has been demonstrated that on the basis of system specific weight there is no advantage to adding filler material to the TES material, filler may be required for other reasons (e.g., to relieve thermal stresses or improve temperature distribution). Referring to figure 9, at cavity temperatures of 2300° and 2400° K, the addition of 10 percent filler ($\alpha = 0.9$) results in an increase in system specific weight of approximately 6 percent while at 2200° K, the weight remains unchanged. Therefore, if required to simplify the fabrication of the TES material specimen, small amounts of filler material may be added with slight attendant increases in specific weight.

In regard to the minimum weights presented in figures 8 and 9 (on the order of 150 lb/kWe), it must be remembered that these are lower than could be achieved on a fully developed flight system. For example, auxiliary hardware such as the collector orientation subsystem, vehicle support structure, and power conditioning equipment is not included in the weight estimates. In addition, it is not possible to anticipate the engineering problems that may arise during the development of such a system and their subsequent effect on weight. Therefore, although suitable for purposes of comparison, these weights are not completely representative of the actual system weight.

SUMMARY OF RESULTS

In summation, the results of the preliminary thermal energy storage - thermionic system study utilizing a one-dimensional steady-state heat-transfer analysis indicate the following:

1. The addition of the metal filler tungsten to the storage material beryllia magnesia, 3 BeO - 2 MgO, does not lower the specific weight of the system.

2. Small amounts of filler may be added to the 3 BeO - 2 MgO to relieve thermal stresses or improve the temperature distribution without increasing the specific weight significantly. For example, at cavity temperatures between 2200° and 2400° K, the addition of 10 percent filler material results in less than a 7 percent increase in system specific weight.

CONCLUDING REMARKS

In order to determine the validity of the steady-state heat-transfer analysis used in this study, a transient heat-transfer analysis was conducted (see appendix B) for a maximum cavity temperature of 2200° K. Values of emitter temperature and solidification

depth (at the end of the dark period) for this case are in good agreement with those obtained from the steady-state approach.

Changes in thermal input and generator temperature during an orbit are considered in appendix C where it is shown that solar flux control is required for the system and that a 6 percent output power variation will be realized during the orbit.

Lewis Research Center,
National Aeronautics and Space Administration,
Cleveland, Ohio, June 9, 1965.

APPENDIX A

SYMBOLS

A	area, cm^2, ft^2, or $in.^2$
C	constant, $W/(cm^2)(^oK)$
D	diameter, cm or ft
H	heat of fusion, (W)(hr)/g
J	diode current density, amp/cm^2
K	concentration ratio
k	thermal conductivity, $W/(cm)(^oK)$
L	length, cm
l	thickness, cm
m	mass, g
n	integer (number of radiation shields)
p	diode power density, W/cm^2
Q	thermal power, W
q	thermal flux, W/cm^2
R	load resistance, ohm
r	reflectivity
SW	specific weight, lb/kWe
T	temperature, ^oK or ^oC
t	orbital time, hr
V	diode output voltage, V
v	volume, cc
W	width, cm
α	ratio of storage material to total material on volumetric basis
β	solar collector misorientation, min
ϵ	emissivity of shield material
η	efficiency, percent
θ	rim angle, deg
ρ	density, g/cc
σ	Stefan-Boltzmann constant
σ'	standard deviation of collector surface errors, deg

Subscripts:

a	aperture
C	cavity
C-A	collector absorber
cs	cross-sectional
D	diode
d	dark time (orbital)
E	emitter
f	filler material
G	generator
g	geometric
i	inner
L	liquid
l	light time (orbital)
MP	melting point
m	temperature exponent
max	maximum
min	minimum
n	integer (number of radiation shields)
o	outer
r	radiating
S	solid

s	storage material
sy	system
TES	thermal energy storage
t	total combination (storage plus filler material)
W	wall

APPENDIX B

TRANSIENT HEAT-TRANSFER ANALYSIS

In estimating the specific weight of a solar thermionic system with thermal energy storage, one-dimensional steady-state heat-transfer equations were considered adequate and the assumption was made that the thermal power delivered to the generator was constant over the entire orbit. In an operating system, the cavity temperature varies continually throughout the orbit, resulting in changes in emitter temperatures and generator input power. It is important in the design of such a system to establish these temperature-time relations, as well as the rate at which the TES material solidifies during the dark period of the orbit. A one-dimensional transient heat-transfer analysis, using the calculational procedures discussed in reference 5, was performed to determine emitter temperature and depth of TES material solidification as a function of orbit position.

In reference 5, the rate at which heat is transferred from the storage material to the thermionic converter is written in general terms of the emitter temperature T_E as

$$q = CT_E^m \tag{B1}$$

where various modes of heat transfer are represented by specifying the values of C and m. In order to establish the heat flux required by the converter, performance data, including power density and efficiency, must be determined as a function of emitter temperature.

Consider a 3 BeO - 2 MgO thermionic system. At the end of the orbit light period, both the cavity and the emitter temperatures are at their maximum values; the emitter temperature reaching the melting point of the storage material (i.e., 2145° K). From the thermionic performance curves of reference 3 (see fig. 6, p. 10), the maximum converter efficiency $\eta_D = 17$ percent, corresponding power density $p = 11.3$ watts per square centimeter, and output voltage $V = 1.2$ volts are obtained for this emitter temperature. To achieve this performance level, a load resistance R of $0.1272/A_E$ ohms, an interelectrode spacing of 2 mils, and a cesium reservoir temperature of 605° K are required for a rhenium emitter - molybdenum collector diode.

Assuming that the converters will operate at fixed load resistance and cesium reservoir temperature throughout the orbit, converter performance data at lower emitter temperatures are determined as follows. The data for a rhenium-molybdenum diode (presented in ref. 6 for interelectrode spacings of 1 and 3 mils) are used and current density and output voltages are obtained at the specified load resistance and reservoir temperature for emitter temperatures of 1850°, 1950°, and 2050° K. Power densities

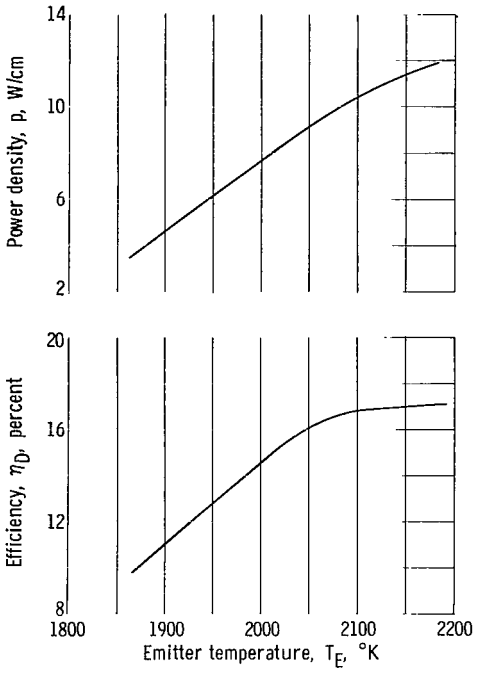

Figure 10. - Converter efficiency and power density plotted against emitter temperature for load resistance optimized at emitter temperature T_E = 2145° K.

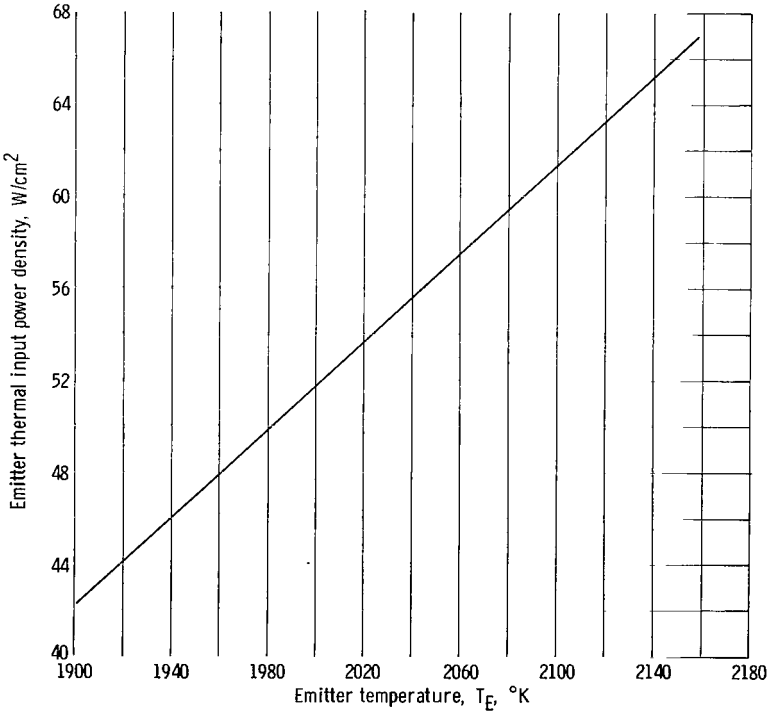

Figure 11. - Required thermal input power density plotted against emitter temperature for fixed load (0.1272/A_E ohm) and cesium reservoir temperature optimized for emitter temperature of 2145° K.

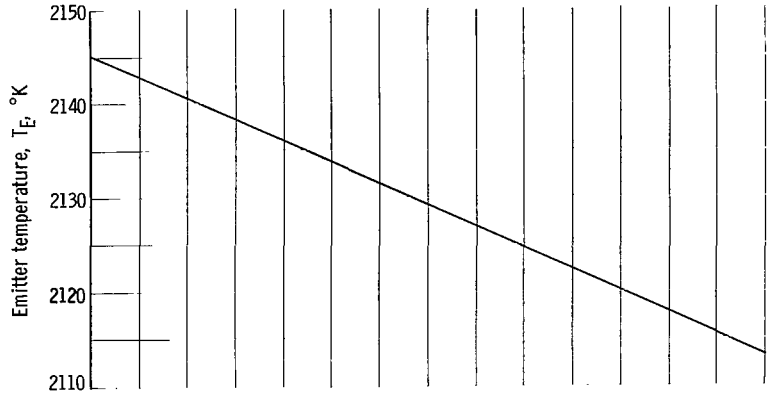

(a) Emitter temperature.

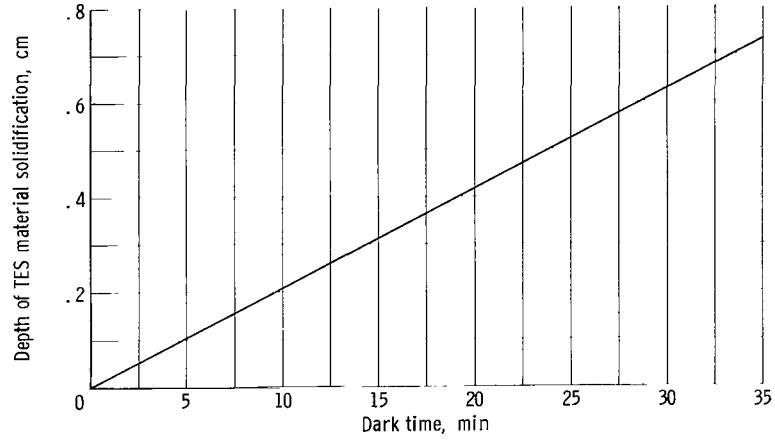

(b) Depth of TES material solidification for 300-mile orbit.

Figure 12. - Emitter temperature and depth of TES material solidification plotted against orbital dark time for maximum cavity temperature of 2200° K and specific load resistance of 0.1272/A_E ohm.

are then determined for a 2-mil spacing by interpolation. Corresponding diode efficiencies are calculated for these emitter temperatures by means of a heat balance method that was found to accurately predict the maximum diode efficiencies presented in reference 3.

The power density and efficiency is plotted as a function of emitter temperatures in figure 10. The heat flux required by the converter p/η_D is, in this case, a linear function of emitter temperature (m = 1, eq. (B1)), as shown in figure 11 with a value of C (eq. (B1)) equal to 1.08×10^{-3} watts per square centimeter per ^{o}K.

After the rate at which heat is rejected by the TES material is established, the results of reference 6 are used to determine the emitter temperature and the depth of the storage-material solidification at any time during the dark period of the orbit. These parameters are presented as a function of time for a 300-mile orbit in figure 12. For the case illustrated, no filler has been added to the storage material (α = 1), and the maximum cavity temperature was taken as 2200^{o} K.

Values of emitter temperature and solidification depth at the end of the dark period, as determined from this analysis, are in very good agreement with the values obtained from the steady-state analyses. For example, the transient analysis gives an emitter temperature of 2113° K and a thermal storage-material thickness of 0.73 centimeter at this operating point, while the corresponding values obtained from the steady-state analysis, modified to include heat capacity effects, are 2111.5° K and 0.769 centimeter. The 5 percent discrepancy in TES material thickness can be attributed to the estimated value of the specific heat used in the transient analysis. It has been determined that for the transient case, a 25 percent change in specific heat results in a 5 percent change in TES material thickness. For the steady-state case, however, a 25 percent change in specific heat changes the TES material thickness by less than 1 percent. Thus a 25 percent error in the estimated value of 3 BeO - 2 MgO specific heat could account for the 5 percent difference between the transient and steady-state value of TES material thickness.

APPENDIX C

THERMAL CONTROL REQUIREMENTS DURING AN ORBIT

In addition to establishing the time dependence of the emitter temperature and TES material solidification depth (appendix B), another important design consideration is the regulation of thermal power that must be provided during the light period. The energy balance analysis described in the following paragraphs was performed to determine the required thermal input and electrical output power as a function of orbital position.

The specific case studied was one in which the maximum cavity temperature was 2200° K and no filler was added to the TES material ($\alpha = 1$). As indicated in table II (p. 13), at the end of the light period the cavity reaches 2200° K with a corresponding emitter temperature of 2145° K, while at the end of the dark period, the cavity temperature is 2145° K and the emitter temperature is 2111° K.

Considering the aforementioned system with a fixed aperture optimized for the maximum cavity temperature (i.e., 2200° K), the thermal power delivered by the solar collector at the beginning and end of the light period is determined from the collector performance curves of figure 5 (p. 9). The net thermal power delivered to each quadrant decreases during the light period from approximately 448 to 440 watts since the increasing cavity temperature results in increased reradiation losses from the absorber. This is shown in the energy diagram presented in figure 13 and table III.

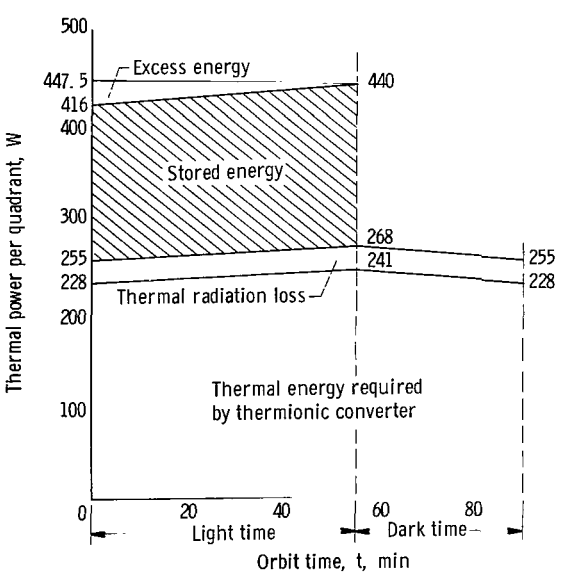

Figure 13. - Thermal power per quadrant plotted against orbit time for maximum cavity temperature $T_{C,\,max}$ = 2200° K, minimum emitter temperature $T_{E,\,min}$ = 2111° K, and converter performance optimized at emitter temperature T_E = 2145° K.

After accounting for the heat absorbed by the storage material and the heat lost by radiation from the outer cavity walls, the thermal power available to each converter at the end of the light period is 241 watts; while at the end of the dark period it is approximately 260 watts. In designing a system, the converter would be sized to accept all the heat available at the end of the light period. Following the approach used in appendix B, the converters are assumed to operate with a fixed load resistance (optimized for $T_E = 2145^{\circ}$ K) and cesium reservoir temperature throughout the orbit. The electrical power density and the heat flux required by the converters at the aforementioned operating conditions are determined from figures 10 and 11, respectively. As the emitter temper-

TABLE III. - GENERATOR THERMAL BALANCE CALCULATIONS

Cavity temperature, T_C, ^oK	Emitter temperature, T_E, ^oK	Wall thermal power, Q_W, W	Diode power density, p, W/cm^2	Diode efficiency, η_D, percent	p/η, W/cm^2	Emitter area,[a] A_E, cm^2	Outer wall radiation loss, Q_r, W	Thermal power used by converter, W	Thermal power rejected per quadrant for balance, W	Total thermal power rejected for balance, W
2145	2111	447.5	10.6	16.9	62.7	3.63	27.3	228	31.5	126
2200	2145	440.0	11.3	17.0	66.5	3.63	26.8	241	0	0

[a]Optimized for $T_E = 2145^o$ K.

ature decreases during the dark period, the thermal power required by the converter decreases from 241 watts at the end of the light period to 228 watts at the end of the dark period (see fig. 13 and table III). Thus, at the beginning of the light period, 31.5 watts per converter or a total of 126 watts must be rejected in order that an energy balance exist. The amount of thermal power that must be rejected decreases to zero at the end of the light period.

If it is assumed that the excess power mentioned previously is rejected (e.g., by a variable generator aperture), the output power variation can be maintained at approximately 5 percent; and the power density decreases from 11.3 watts per square centimeter, ($J = 9.42$ amp/cm^2, $V = 1.2$ V) at $T_E = 2145^o$ K to 10.6 watts per square centimeter, ($J = 9.13$ amp/cm^2, $V = 1.16$ V) at $T_E = 2111^o$ K.

REFERENCES

1. Batutis, E. F.; and Purdy, D. L.: Thermal Energy Storage for Thermionic Conversion. I - Materials for Thermal Energy Storage. II - Thermal Energy Storage Systems Considerations. Paper No. 2505-62, ARS, 1962.

2. Menetrey, W. R.; and Smith, A.: Solar Energy Thermionic Conversion System. Paper No. 2499-62, ARS, 1962.

3. Kitrilakis, S. S.; Meeker, M. E.; and Rasor, N. S.: Annual Technical Summary Report for the Thermionic Emitter Materials Research Program, July 1-June 30, 1962. Rept. No. 2-63, Thermo Electron Eng. Corp., 1962.

4. Stephens, Charles W.; and Haire, Alan M.: Internal Design Considerations for Cavity-Type Solar Absorbers. ARS J., vol. 31, no. 7, July 1961, pp. 896-901.

5. Cullom, Richard R.; Robbins, William H.; and Todd, Carroll, A.: One-Dimensional Heat-Transfer Analysis of Thermal-Energy Storage for Solar Direct-Energy-Conversion Systems. NASA TN D-2119, 1964.

6. Kitrilakis, S. S.; and Weinstein, J. H.: Second Technical Summary Report for the Thermionic Emitter Materials Research Program, July 1, 1962-Sept. 30, 1963. Rept. No. 27-64, Thermo Electron Eng. Corp., 1963.

7. Goldsmith, Alexander; Waterman, Thomas E.; and Hirschhorn, Harry J.: Thermophysical Properties of Solid Materials. Vol. I - Elements. Rept. No. TR-58-476, WADD, Aug. 1960.

3/12/85

"The aeronautical and space activities of the United States shall be conducted so as to contribute . . . to the expansion of human knowledge of phenomena in the atmosphere and space. The Administration shall provide for the widest practicable and appropriate dissemination of information concerning its activities and the results thereof."

—NATIONAL AERONAUTICS AND SPACE ACT OF 1958

NASA SCIENTIFIC AND TECHNICAL PUBLICATIONS

TECHNICAL REPORTS: Scientific and technical information considered important, complete, and a lasting contribution to existing knowledge.

TECHNICAL NOTES: Information less broad in scope but nevertheless of importance as a contribution to existing knowledge.

TECHNICAL MEMORANDUMS: Information receiving limited distribution because of preliminary data, security classification, or other reasons.

CONTRACTOR REPORTS: Technical information generated in connection with a NASA contract or grant and released under NASA auspices.

TECHNICAL TRANSLATIONS: Information published in a foreign language considered to merit NASA distribution in English.

TECHNICAL REPRINTS: Information derived from NASA activities and initially published in the form of journal articles.

SPECIAL PUBLICATIONS: Information derived from or of value to NASA activities but not necessarily reporting the results of individual NASA-programmed scientific efforts. Publications include conference proceedings, monographs, data compilations, handbooks, sourcebooks, and special bibliographies.

Details on the availability of these publications may be obtained from:

SCIENTIFIC AND TECHNICAL INFORMATION DIVISION

NATIONAL AERONAUTICS AND SPACE ADMINISTRATION

Washington, D.C. 20546